

Pinpointing the peripheral bias in neural scene-processing networks during natural viewing

Christopher Baldassano

Princeton Neuroscience Institute, Princeton University,
Princeton, NJ, USA



Li Fei-Fei

Department of Computer Science, Stanford University,
Stanford, CA, USA



Diane M. Beck

Department of Psychology and Beckman Institute,
University of Illinois at Urbana–Champaign,
Champaign, IL, USA



Peripherally presented stimuli evoke stronger activity in scene-processing regions than foveally presented stimuli, suggesting that scene understanding is driven largely by peripheral information. We used functional MRI to investigate whether functional connectivity evoked during natural perception of audiovisual movies reflects this peripheral bias. For each scene-sensitive region—the parahippocampal place area (PPA), retrosplenial cortex, and occipital place area—we computed two measures: the extent to which its activity could be predicted by V1 activity (connectivity strength) and the eccentricities within V1 to which it was most closely related (connectivity profile). Scene regions were most related to peripheral voxels in V1, but the detailed nature of this connectivity varied within and between these regions. The retrosplenial cortex showed the most consistent peripheral bias but was less predictable from V1 activity, while the occipital place area was related to a wider range of eccentricities and was strongly coupled to V1. We divided the PPA along its posterior–anterior axis into retinotopic maps PHC1, PHC2, and anterior PPA, and found that a peripheral bias was detectable throughout all subregions, though the anterior PPA showed a less consistent relationship to eccentricity and a substantially weaker overall relationship to V1. We also observed an opposite foveal bias in object-perception regions including the lateral occipital complex and fusiform face area. These results show a fine-scale relationship between eccentricity biases and functional correlation during natural perception, giving new insight into the structure of the scene-perception network.

comparisons between eccentricity preference and category selectivity revealed a surprising correspondence between these low- and high-level properties, with face and object regions driven more by foveal stimulation, and scene regions (Epstein, 2014) by peripheral stimulation (Hasson, Levy, Behrmann, Hendler, & Malach, 2002; Levy, Hasson, Avidan, Hendler, & Malach, 2001). These results suggested an intimate relationship between category selectivity and eccentricity preference, linked by innate cortical structure (Kanwisher, 2001) and/or acuity demands (Malach, Levy, & Hasson, 2002). More recent work has confirmed this retinotopic organization of high-level cortex (Goesaert & Op de Beeck, 2010; Huang & Sereno, 2013) and identified peripherally biased field maps overlapping with scene regions (Arcaro, McMains, Singer, & Kastner, 2009). The peripheral bias in scene-sensitive regions is also reflected in behavior, since subjects show superior recognition in the periphery for certain scene properties (Boucart, Moroni, Thibaut, Szaffarczyk, & Greene, 2013; Larson, Freeman, Ringer, & Loschky, 2014; Larson & Loschky, 2009).

Studies of eccentricity dependence of higher level visual regions have generally relied on eccentricity-controlled stimuli (i.e., requiring fixation), using checkerboard rings (Arcaro et al., 2009), rings of objects (Goesaert & Op de Beeck, 2010; Hasson et al., 2002; Levy et al., 2001), or a moving annulus window over a natural movie (Huang & Sereno, 2013). Real-world perception, however, differs markedly from these stimuli, since objects and scene structures stretch across both foveal and peripheral eccentricities, and the retinal image changes in a structured way over time due to

Introduction

Visual receptive-field position is one of the organizing principles of visual processing in the brain. Early

Baldassano, C., Fei-Fei, L., & Beck, D. M. (2016). Pinpointing the peripheral bias in neural scene-processing networks during natural viewing. *Journal of Vision*, 16(2):9, 1–14, doi:10.1167/16.2.9.

doi: 10.1167/16.2.9

Received March 3, 2016; published May 17, 2016

ISSN 1534-7362



both events in the world and eye movements. Under these naturalistic conditions, it is not known how information from different eccentricities propagates to higher level visual regions, or whether eccentricity dependence is even detectable.

To circumvent the need for controlled and unnatural viewing conditions, we turned to functional connectivity, which can be computed under natural viewing conditions and during eye movements. Regions with similar eccentricity properties have been shown to be strongly functionally connected, both within early visual cortex (Arcaro, Honey, Mruczek, Kastner, & Hasson, 2015; Baldassano, Iordan, Beck, & Fei-Fei, 2012; Bock et al., 2015; Heinzle, Kahnt, & Haynes, 2011) and between hV4 and higher level category-specific regions (Baldassano et al., 2012). We therefore make the assumption that those regions of the brain that are primarily driven by peripheral representations will mirror the activity of (i.e., will be functionally connected to) peripheral representations in V1 (regardless of the visual input or where the eyes are pointing), whereas those areas that are driven more by foveal representations will show tighter coupling with the activity in foveal regions of V1. Thus, rather than compare conditions in which only foveal or peripheral stimulation is present, we can use data from subjects who were freely viewing intact movie clips. Because these analyses are stimulus independent, we have the ability to combine data from many data sets in which subjects are viewing time-varying visual stimuli rather than being restricted to a single controlled stimulus.

Previous work on topographies of functional connectivity has largely relied on discrete binning of foveal and peripheral connections (Arcaro et al., 2015), which leads to very coarse approximations of eccentricities (if large bins are used) or can lead to poor signal-to-noise ratios (if small bins are used). Instead, we use a specialized method to estimate smooth connectivity maps (Baldassano et al., 2012). We show that this sensitive analysis not only identifies more peripherally and foveally connected vertices or voxels but also allows us to examine more fine-grained structure within scene regions and relationships between different pairs of regions. As we will show, this approach uncovers a distributed network involved in peripheral visual processing that overlaps with scene-sensitive networks.

Methods

Participants

Fifteen subjects (seven female, eight male; ages 24–34 years) with normal or corrected-to-normal vision freely viewed movie stimuli while imaging data was

acquired. The study protocol was approved by the Princeton University Institutional Review Board, and all subjects gave their written informed consent.

Experimental stimuli

Subjects watched a variety of natural movies, with total acquisition times ranging from 8 to 50 min across subjects. Ten subjects viewed a portion of the movie *Dog Day Afternoon* (including audio), as described in a previous publication (Arcaro et al., 2015); note that we used free-viewing runs (rather than the fixation runs analyzed previously). Eight of these subjects watched a 5-min clip six times: twice unaltered from the original movie, twice with coarse temporal reordering (randomly ordered movie segments of 7–20 s), and twice with fine temporal reordering (randomly ordered movie segments of 0.5–1.5 s). One subject viewed only the two unaltered runs of the clip, and one viewed the clip once in each condition. The remaining five subjects watched other clips also taken from popular movie and television shows: One watched a 25-min episode of *The Twilight Zone* titled “The Lateness of the Hour” (1960; Chen, Honey, Simony, Arcaro, Norman, & Hasson, 2015); two watched a 50-min segment from the episode “A Study in Pink” of BBC’s *Sherlock* (2010; Chen, Leong, Norman, & Hasson, 2016); one watched a 26-min segment from an episode of BBC’s *Merlin* (2008); and one watched a 4-min clip from Charlie Chaplin’s 1921 *The Kid* twice. We note that the variety of movies used ensures that our connectivity measures are not driven by a specific stimulus, and instead reflect a more general pattern of connectivity.

Functional MRI (fMRI) acquisition and preprocessing

A gradient echo, echo planar sequence was used to acquire data from the whole brain, with an in-plane spatial resolution of 3×3 mm (field of view: 192×192 mm), a slice thickness of 4 mm (27 slices), and a repetition time of 1.5 s (for full details, see Arcaro et al., 2015). In addition, a high-resolution anatomical image at an isotropic resolution of approximately 1 mm was collected for each subject.

Data were minimally preprocessed using the FsFast analysis stream from Freesurfer (Dale, Fischl, & Sereno, 1999; Fischl, Sereno, & Dale, 1999). Each run was corrected for head motion, registered to the subject’s anatomical image, and then resampled both into MNI volume space and onto the subject’s cortical surface using the vertices of the fsaverage6 mesh (no explicit spatial smoothing was applied). Our spatial units of study are therefore surface vertices rather than

volume voxels. The data were then imported into MATLAB (The MathWorks Inc., Natick, MA), and we regressed out time-course components related to motion (three translation and three rotation components), the average signal in deep white matter (at least 3 voxels from gray matter), and linear drift. A high-pass filter with a cutoff of 150 s was applied to remove slow drift, and then each vertex's time course was converted to a z-score. Finally, we regressed out the global signal averaged over all gray-matter vertices, which has been shown to increase the specificity of functional correlations between regions (Fox, Zhang, Snyder, & Raichle, 2009).

Retinotopic mapping and regions of interest

The borders of V1 and the eccentricity preferences for V1 vertices were measured in each individual subject using a traveling-wave paradigm (Swisher, Halko, Merabet, McMains, & Somers, 2007), with four or five runs for polar angle and two or three runs for eccentricity (with logarithmically scaled eccentricity steps). Due to limitations imposed by the scanner display, the mapping stimuli did not extend beyond 15° eccentricity. V1 was defined as the region above and below the calcarine fissure, delineated ventrally and dorsally by the presence of a vertical meridian and anteriorly by the end of the peripheral maps. The log eccentricity of each vertex was defined by computing the phase of its response to the eccentricity traveling wave (at the wave frequency), which was then exponentiated and scaled to the range of 0° to 15°.

All but one of the subjects had previously participated in a standard category localizer experiment (Mruczek, von Loga, & Kastner, 2013) to define category regions of interest (ROIs) including the lateral occipital complex (LOC), fusiform face area (FFA), parahippocampal place area (PPA), occipital place area (OPA, also known as the transverse occipital sulcus), and retrosplenial cortex (RSC). Fourteen subjects had individual PPA, FFA, and LOC ROIs in at least one hemisphere, and eight had individual OPA and RSC maps. For retinotopic regions beyond V1 (notably PHC1 and PHC2), a group-level maximum probability atlas was used (Wang, Mruczek, Arcaro, & Kastner, 2014). This allowed the definition of the anterior PPA (aPPA) as the portion of PPA anterior to PHC2 in 13 subjects.

Connectivity analyses

Our goal was to determine which specific portion of V1 is most functionally connected to a seed ROI elsewhere in the brain. Possible approaches based on

previous work include correlating the seed ROI's time course with each individual surface vertex in V1 (Butt, Benson, Datta, & Aguirre, 2013) or with the average time courses of V1 eccentricity bins (Arcaro et al., 2015). Instead, we can improve our statistical power and avoid discrete bins by treating vertex-level connectivity as a multiple-regression problem (Baldassano et al., 2012), in which we attempt to describe the average time course from a seed region as a linear weighted combination of time courses of V1 vertices (from both hemispheres; Figure 1a). Every vertex is assigned a weight in this regression, which indicates how much unique information about the seed time course is present in this particular vertex. For example, if the seed time course is related only to activity in peripheral V1, then only peripheral V1 vertices will receive nonzero weights. In addition to the map of fitted weights, we can gain additional insight by looking at the degree of fit, measured as the fraction of variance in the seed ROI that could be explained by this optimal combination of V1 time courses. We refer to this as the *connectivity strength* between V1 and the seed ROI, since it measures the degree to which the seed ROI is functionally correlated with signals within V1. If a seed region is totally unrelated to V1, it will have a connectivity strength near zero, since it will not be possible to predict its activity from V1 activity. We note that with this analysis, it is possible to observe a strong bias (i.e., clear relative differences in the peripheral versus central weights) but weak connectivity strength (i.e., the V1 model captures little of the variance in the seed area overall), or vice versa.

In this data set, as in most fMRI data sets, we do not have enough data to perform this regression without incorporating some prior knowledge. In fact, since the number of V1 surface vertices (and hence the number of weights we are trying to learn) exceeds the number of time points for some subjects, it is not even possible to construct the pseudoinverse required for the least-squares normal equations (i.e., the problem is highly underconstrained and ill posed). In keeping with the known retinotopic gradients in V1 and the smoothness of the blood-oxygen-level-dependent signal more generally, we solved this problem by enforcing spatial smoothness, requiring that adjacent vertices be assigned similar weights in the regression. This smoothness prior can be viewed as a compromise between methods without any spatial constraints, which require large amounts of training data (Heinze et al., 2011), and connective field methods that specify a receptive-field shape, losing flexibility (Haak et al., 2013). The full optimization objective can be written as

$$\min_w \|V \cdot w - s\|_2^2 + \lambda \sum_{i=1}^N \sum_{j \in n_i} \frac{(w_i - w_j)^2}{|n_i|},$$

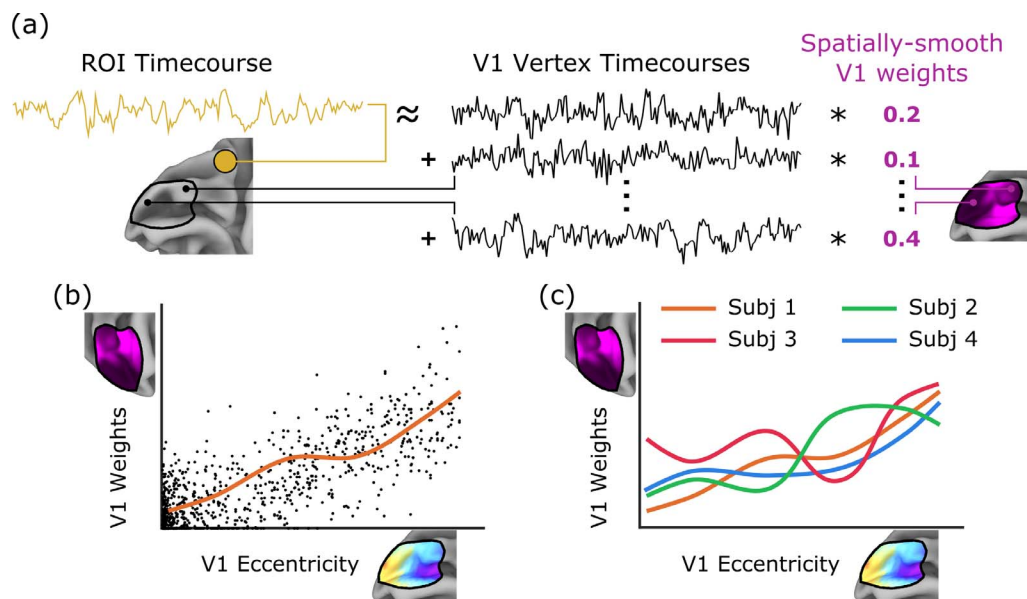


Figure 1. Measuring the eccentricity profile of connectivity to V1. (a) Given the mean time course from a region of interest (or searchlight), we fit a set of weights over V1 vertices (purple) such that the weighted average of the V1 time courses best approximates the ROI time course. We refer to the goodness of fit (fraction of ROI time-course variance explained by V1) as the V1 *connectivity strength* for this ROI. (b) We then compare the fitted weight at each V1 vertex to its independently defined eccentricity preference. The smoothed *connectivity profile* of weights versus eccentricity indicates which V1 eccentricities are most strongly connected to the ROI time course. For example, this connectivity profile (orange) would indicate stronger connectivity to peripheral than foveal V1. (c) We measure the consistency of these profiles across subjects, to determine if an ROI shows a consistent functional connection to particular eccentricities.

where w is the V1 connectivity weight vector, V is the matrix of V1 time courses, s is the seed time course, N is the number of V1 vertices, and n_i is the set of spatial neighbors of vertex i . The first term implements a standard least-squares multiple regression, while the second term penalizes weight differences for neighboring vertices; see our full paper (Baldassano et al., 2012) for additional description.

The overall level of smoothing is controlled via a hyperparameter λ , which interpolates between no smoothing ($\lambda = 0$) and a constant weight map over the whole ROI ($\lambda = \infty$). However, note that even for a particular choice of λ , the strength of the spatial smoothness can vary locally over V1, with weights changing faster in some regions than others depending on the underlying signals' similarity to the searchlight time course. This is a major advantage over pre-smoothing the data with a fixed Gaussian kernel, which would force us to pick a fixed amount of spatial smoothing that is constant through all of V1. The λ parameter therefore only sets a rough spatial scale over which we would like the weight maps to vary. In all experiments in this article, we use $\lambda = 1000$, in order to yield maps that are smooth on the scale of about 5–10 mm (Supplementary Figure S1). A precise setting of λ is not required to obtain the eccentricity preference results we report, as shown in Supplementary Figure S2.

In this work we specifically restricted the weights to be positive; negative weights in multiple regression can be challenging to interpret, especially after global signal regression (Murphy, Birn, Handwerker, Jones, & Bandettini, 2009). The regularized regression problem (with nonnegative weight constraint) is a simple quadratic program, which we solve using two passes of MATLAB's quadprog. We first used the interior-point solver to obtain an approximate solution, and then applied the trust-region solver to refine the weights. Please see <https://www.bitbucket.org/cbaldassano/voxel-level-functional-connectivity> for publicly available MATLAB code.

After fitting a map of V1 connectivity weights, we examined the relationship between these weights and the independently measured eccentricity preferences within V1 determined from retinotopic mapping (Figure 1b). We can summarize this relationship by calculating the average weight as a function of eccentricity. For every eccentricity, we compute the average weight in a small neighborhood around this eccentricity (using a Gaussian kernel with standard deviation equal to 10% of the full eccentricity range). This yields a *connectivity profile* over V1, describing which eccentricities in V1 are most related to the time course of this ROI in this subject. For example, the connectivity profile in Figure 1b (in orange) shows that weights generally increase with eccentricity, indicating

a bias toward peripheral connectivity. We can test these eccentricity profiles for foveal versus peripheral preference by computing the Pearson correlation between weights and eccentricity; positive values indicate a peripheral bias (weights increasing with eccentricity), while negative values indicate a foveal bias (weights decreasing with eccentricity).

Searchlight and statistical analyses

A searchlight analysis was performed for each subject. We selected a center vertex on the subject's cortical surface and defined a small searchlight region as all vertices fewer than 5 faces away (approximately 7 mm away) from the center along the cortical sheet. To reduce computation time, rather than centering a searchlight on each of the $\sim 80,000$ surface vertices we randomly selected searchlights in each subject such that every vertex was included in at least one searchlight (yielding approximately 2,600 searchlights per subject).

The vertex time courses within the searchlight were averaged together to produce a single searchlight time course. We then applied our connectivity method as with the ROIs, yielding a connectivity strength (how well this searchlight's activity could be predicted by V1 activity), a profile of weights as a function of eccentricity, and the linear correlation between weights and eccentricity; the latter is used to indicate foveal or peripheral eccentricity bias. Results for each vertex were calculated by averaging the results from all searchlights overlapping that vertex. For comparison purposes, we also binned the V1 vertices by eccentricity, into foveal ($\sim 0^\circ\text{--}1^\circ$), parafoveal ($\sim 1^\circ\text{--}5^\circ$), and peripheral ($\sim 5^\circ\text{--}15^\circ$) thirds with equal numbers of vertices in each. We measured the correlation between the searchlight time course and the mean time courses in each of these bins.

Finally, we determined which profiles and correlations were consistent across subjects (Figure 1c). For the profiles, we measured their consistency across subjects in a manner similar to that used for computing time-course similarities across subjects (Regev, Honey, Simony, & Hasson, 2013). Each subject's profile (for a particular ROI or searchlight vertex) was correlated with the mean profile of all other subjects, and then these correlation values were averaged together. If all subjects have a similar profile, then this intersubject correlation will be high, whereas it will be close to zero if subjects have unrelated profiles. We used a permutation test to determine a significance threshold, creating a null searchlight map in which the vertex correspondence was shuffled across subjects. In this null map, the consistency of a vertex in the group map was computed as the average of consistencies from 15 random vertices, one from each subject. No vertex

should have a high consistency value in this map, since each is an average of vertices drawn from random parts of the brain across subjects. Pooling across all $\sim 80,000$ vertices, this produced a null distribution that estimated the likelihood that a high consistency value could occur due to chance. For each vertex and in each ROI, we compared its profile consistency to this null distribution and computed a p value as the fraction of null consistencies that were at least as large. This p value therefore represents the probability that a consistency value could have been generated by a random draw of 15 eccentricity profiles. For detecting differences between profiles, we also constructed a null distribution by computing all differences between consistencies in the null map, and defined a p value as the fraction of null differences whose absolute consistency difference was at least as large as the true profile difference. Linear correlations of weight versus eccentricity were Fisher transformed and then subjected to a t test; one-sided t tests were used in the ROIs (based on previous work identifying LOC and FFA as foveal and OPA, RSC, and PPA as peripheral), whereas two-sided t tests were used in the searchlight. For the binning analysis, the correlation in each bin was compared to the mean correlation in the other two bins with a one-sided t test. Searchlight p values were corrected for multiple comparisons using the false discovery rate (q), calculated with the same calculation as AFNI's 3dFDR (Cox, 1996).

Results

For each visual ROI, we computed a map of weights over V1 such that the weighted average V1 time course predicted the ROI's mean time course as closely as possible. Regions of V1 with high weights are most predictive of, and therefore most functionally related to, activity in the ROI. Having a fine-grained map of connectivity with V1, we can compare the map of V1 weights to the subject-specific map of eccentricity preferences in V1 (as determined by the retinotopic mapping procedure) to determine if the ROI is preferentially connected to specific V1 eccentricities.

Results for all major scene ROIs are shown in Figure 2 (left column). OPA, PPA, and RSC all have weight-versus-eccentricity profiles that are consistent across subjects (all $ps < 0.001$ by permutation test) and show a marked connectivity preference for portions of V1 beyond 5° of eccentricity. This peripheral bias is revealed by a highly significant and positive linear trend of weight versus eccentricity in each ROI—OPA: $t(7) = 3.59$, $p = 0.004$; PPA: $t(13) = 6.49$, $p < 0.001$; RSC: $t(7) = 6.69$, $p < 0.001$ (one-tailed t test). The results also reveal some differences among the regions. OPA shows

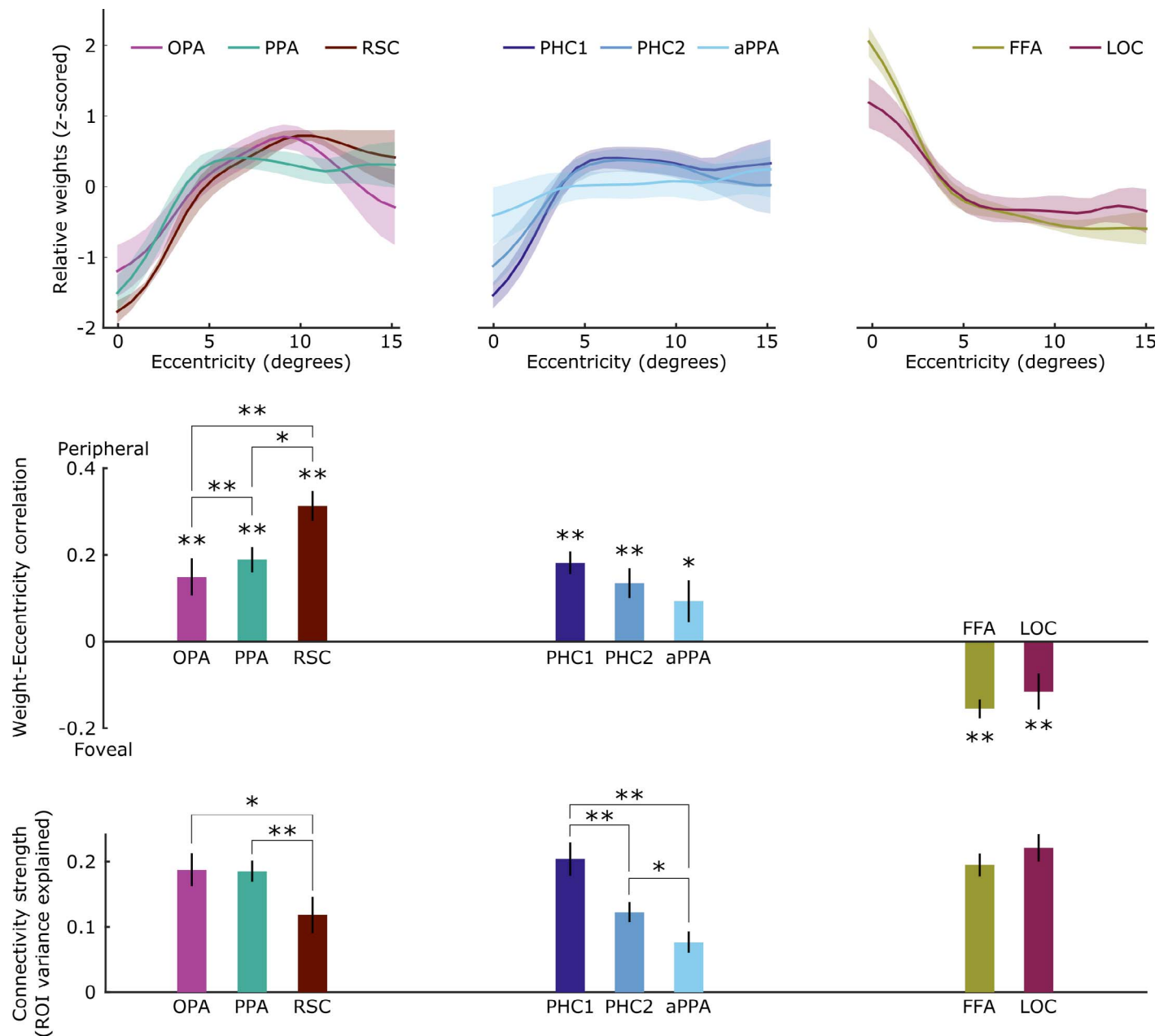


Figure 2. Connectivity properties for category-selective ROIs. (Top) For each ROI, the z-scored weight-versus-eccentricity connectivity profile was averaged across all subjects. All scene-sensitive regions (OPA, PPA, and RSC) show a sharp increase in V1 connectivity as we move outside of 5° of eccentricity. Within PPA, PHC1 and PHC2 show similar profiles, while aPPA has a much less pronounced eccentricity preference. FFA and LOC show the opposite behavior, with connectivity weights concentrated on foveal eccentricities less than 5° . (Middle) We can test whether weights in each ROI increase or decrease with increasing eccentricity by measuring the linear correlation between fitted weights and eccentricity. OPA, PPA, and RSC all connect consistently to more peripheral portions of V1, with the strongest peripheral biases in PPA and especially RSC. There is a detectable peripheral bias throughout all subregions of PPA, though it is weak in aPPA. V1 weights indicating connectivity to FFA and LOC correlate negatively with eccentricity, indicating a foveal connectivity preference. (Bottom) A substantial portion of the variance in visual ROIs can be predicted by a weighted average of V1 time courses, but OPA and PPA are significantly more coupled to V1 than RSC. There is a sharp gradient across PPA, with more posterior subregions highly related to V1 activity and more anterior subregions less predictable from V1.

peak connectivity around 10° of visual angle, while PPA and RSC maintain high weights out to the maximum eccentricity measured (15°), and hence OPA shows a weaker overall linear trend between weight and

correlation—PPA > OPA: $t(8) = 5.22$, $p = 0.001$; RSC > OPA: $t(8) = 4.14$, $p = 0.004$ (two-tailed t test). In addition, RSC shows a more pronounced weight difference between foveal and peripheral eccentricities

compared to PPA, and has a stronger weight–eccentricity correlation—RSC > PPA: $t(8) = 2.74$, $p = 0.029$ (two-tailed t test). We note that many of these subtler effects, and particularly the detailed information about peak connectivity and eccentricity, would be lost in methods that use fixed foveal versus peripheral stimulation (Hasson et al., 2002) or fixed bins across V1 (as in our comparison bin analysis later).

Another difference among the scene regions is in their overall degree of coupling, or connectivity strength, with V1. To measure how strongly each ROI time course is related to V1 activity, we measured the fraction of variance in the ROI time course that could be explained by the weighted combination of V1 time courses. This connectivity strength is substantial (greater than 10%) for all scene regions, but significantly higher in OPA and PPA than RSC—OPA > RSC: $t(8) = 2.80$, $p = 0.027$; PPA > RSC: $t(8) = 7.97$, $p < 0.001$ (two-tailed t test)—indicating that a smaller portion of RSC’s activity can be predicted purely by V1 activity.

Based on our previous work (Baldassano, Beck, & Fei-Fei, 2013, 2015), we segmented PPA into three subregions, corresponding to retinotopic maps PHC1 and PHC2 and a region anterior to these maps (aPPA). As in the aforementioned ROI analyses, weight maps were learned separately based on the mean time course within each of these subregions (Figure 2, middle column). PHC1 and PHC2 show weight profiles that are consistent across subjects ($p < 0.001$ by permutation test) and more strongly connected to peripheral than foveal eccentricities. The connectivity profile for aPPA, however, is not very correlated across subjects ($p > 0.1$ by permutation test), indicating that this region has a much less well-defined preference for specific eccentricities; aPPA’s connectivity profile is significantly less consistent than that of PHC1 ($p < 0.001$, permutation test) and PHC2 ($p < 0.02$, permutation test). When testing simply for a linear correlation between weights and eccentricity, it is possible to detect a peripheral bias in all three subregions—PHC1: $t(14) = 6.96$, $p < 0.001$; PHC2: $t(14) = 3.83$, $p < 0.001$; aPPA: $t(12) = 2.08$, $p = 0.030$ (one-tailed t test)—including a weak peripheral preference in anterior PPA. There is an even larger difference between the subregions in V1 connectivity strength, with PPA subregions becoming less and less predictable from V1 activity as we move posterior to anterior—PHC1 > PHC2: $t(13) = 4.42$, $p < 0.001$; PHC1 > aPPA: $t(13) = 4.53$, $p < 0.001$; PHC2 > aPPA: $t(13) = 2.85$, $p = 0.014$ (two-tailed t test). It is unlikely that this gradient is driven by local noise correlations, since V1 and PHC1 are separated by more than 25 mm.

For comparison, we also fitted V1 connectivity maps for FFA and LOC, and saw opposite effects compared to those of the scene regions. Both of these regions had

weight profiles that were consistent across subjects ($p < 0.001$ by permutation test) but had weights that were highly concentrated within 5° of eccentricity. A linear correlation of weights versus eccentricity was significantly negative in both regions—FFA: $t(13) = 7.78$, $p < 0.001$; LOC: $t(13) = 2.81$, $p = 0.007$ (one-tailed t test)—indicating that weights decreased at higher eccentricities. Both regions were strongly coupled to V1 activity, with connectivity strengths similar to those of OPA and PPA. Together, our ROI results indicate that examining fine-grained connectivity patterns over V1 reveals new insights compared to simply measuring overall correlations between V1 and regions of interest.

Moreover, computing a separate bias measure and connectivity-strength measure allows for further understanding of the network. Note that there is no simple relationship between V1 connectivity strength and eccentricity preference. For example, RSC has a very strong peripheral bias but relatively low V1 connectivity strength, while aPPA shows both weak peripheral bias and weak V1 connectivity. Regions with similar V1 connectivity strength (e.g., PPA and LOC) can also have strong eccentricity biases in opposite directions (peripheral and foveal, respectively).

We performed this same set of analyses in a surface-based searchlight, to explore regions throughout the cortex that had V1 connectivity patterns with a consistent eccentricity preference. Colored vertices in Figure 3 are those whose weight-versus-eccentricity profiles were consistently correlated across subjects (i.e., had a consistent bias to any range of eccentricities), and the vertex color indicates the position of the peak of the eccentricity profile (averaged across subjects). Vertices in red had connectivity profiles that were highest at foveal eccentricities, indicating that they were most correlated with foveal V1 in all subjects. Similarly, yellow and green vertices were most connected to parafoveal eccentricities, and blue and purple vertices were connected to the most peripheral eccentricities covered by our stimuli. Note that we are not yet considering the connectivity strength of these vertices; colored vertices may have very low correlations to all of V1 but still show a significant bias (i.e., significant difference in connectivity to different eccentricities).

We observed topographies of eccentricity preference spanning large portions of the brain, which are consistent with known retinotopic maps but also extend into more anterior regions. Foveal connectivity is observed extending from the foveal confluence in early visual cortex down the ventral visual stream (including LOC and FFA) into the anterior temporal lobe and up into the superior temporal sulcus, and is present near the intersection of V3a, V3b, and IPS0. A foveal preference is also observed in lateral and orbital prefrontal cortex, and in a small patch in the medial parietal lobe anterior to left RSC. Peripheral connec-

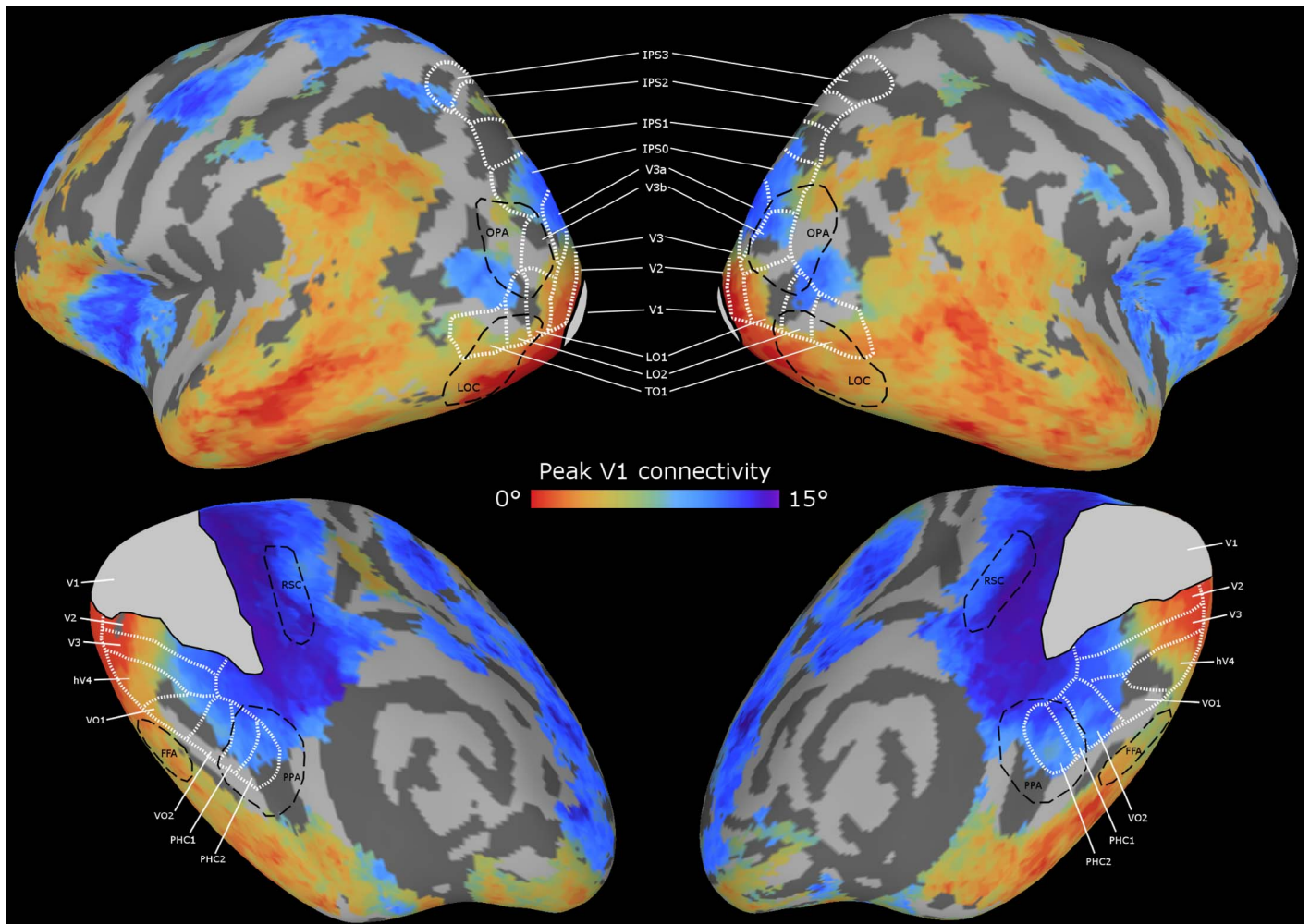


Figure 3. Peak of learned weight profiles. A weight-versus-eccentricity profile (as in Figure 2, top) was computed in a searchlight across the surface of all subjects. Colored vertices are those that showed correlated profiles across subjects ($q < 0.01$ by permutation test, minimum cluster size = 100 mm²). Foveal connectivity extends from the foveal confluence down the ventral visual stream and into the superior temporal sulcus, and also appears near the intersection of V3a, V3b, and IPS0 as well as in ventrolateral prefrontal cortex. Peripheral connectivity wraps around from the collateral sulcus to the superior occipital lobe and is also present in medial prefrontal cortex, precentral cortex, and the insula.

tivity, by contrast, shows a very different large-scale pattern. A band of peripherally connected vertices wraps around visual cortex from PPA, through RSC, to OPA, covering all major regions of scene-selective cortex. Peripheral connectivity is also present throughout the medial frontal lobe, around the central sulcus, and in the insula.

As in the ROI analysis, we also performed a searchlight analysis in which we tested for vertices whose weight maps simply show an overall linear trend with eccentricity (indicating that connectivity is either increasing or decreasing with eccentricity). This approach has the advantage of providing an easy metric for identifying a peripheral versus foveal bias, but the disadvantage of obscuring interesting subtleties in the data: It will fail to find vertices that have preferences for intermediate eccentricities and ignores the precise

shape of the eccentricity profiles. Nonetheless, this analysis identifies strongly peripheral and foveal regions that are consistent with our main analysis (see Supplementary Figure S3).

Our main searchlight analysis also yielded a map of V1 connectivity strength for each vertex (the fraction of its variance that could be explained by the weighted V1 average time course). As shown in Figure 4, all of visual cortex had activity that was strongly related to V1 signals. This coupling gets weaker as we move to more anterior regions, with a steep drop-off around RSC and within the PPA. For parietal, anterior temporal, and frontal lobes, very little of the time-course variance is related to V1. This is not inconsistent with the existence of eccentricity preferences in these regions as observed in Figure 3; these regions are correlated to some

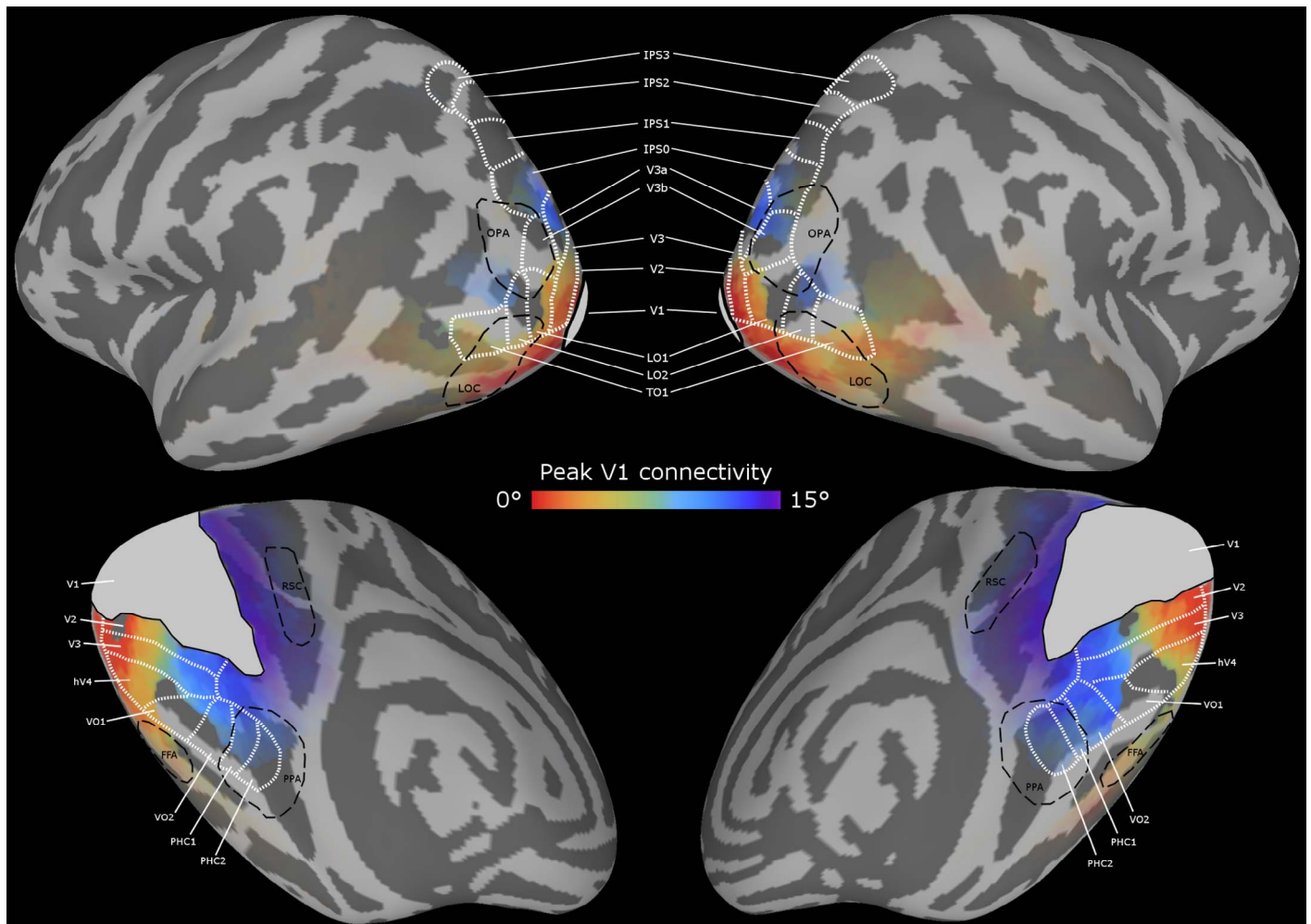


Figure 4. Connectivity strength to V1. For vertices showing a significant dependence on V1 eccentricity (Figure 3), we measured their connectivity strength to V1, defined as the fraction of time-course variance that could be explained by the weighted average of V1 time courses. As in Figure 3, hue represents eccentricity bias. Transparency of that color overlay indicates the connectivity strength, with fully opaque vertices having at least 30% of their time course predicted by V1 activity. Early visual regions, LOC, FFA, and parts of OPA are strongly related to V1, but this relationship drops off rapidly around RSC and within PPA. Very little of the activity in regions anterior to the superior temporal sulcus was related to V1 activity, indicating that although they connect consistently to a particular portion of V1 (Figure 3), this coupling is relatively weak.

portions of V1 significantly more than other portions of V1, but these correlations are low overall.

We chose to perform our analysis by fitting a smoothly varying connectivity map over V1 in order to be as sensitive as possible to potentially subtle connectivity patterns, but we expected that a more traditional binning-based analysis (Arcaro et al., 2015) would yield a similar result, albeit with reduced sensitivity and less precise estimates of the peak eccentricity preferences in each region. To confirm this intuition, we performed a comparison analysis in which we averaged the time courses of V1 vertices within three bins based on eccentricity (with equal numbers of vertices in each bin). The eccentricities within each bin varied slightly across subjects, but consisted approximately of a foveal bin (0° – 1°), a parafoveal bin (1° – 5°),

and a peripheral bin (5° – 15°). As in the previous analysis, we conducted a searchlight over the entire cortical surface, now calculating the correlation between each of the three V1 bin time courses and the average time course in the searchlight. We identified vertices whose correlation to one of the bins was significantly greater than the average correlation to the other two, across subjects. As shown in Figure 5, this analysis yields a map that matches the broad topography found in our analysis (compare to Figure 3), with foveal connectivity in ventral occipitotemporal cortex, the superior temporal sulcus, orbital prefrontal cortex, and anterior to RSC, and with parafoveal or peripheral connectivity in scene regions, medial frontal cortex, the central sulcus, and the insula. Our regression analysis, however, is substantially more sensitive, yielding 51%

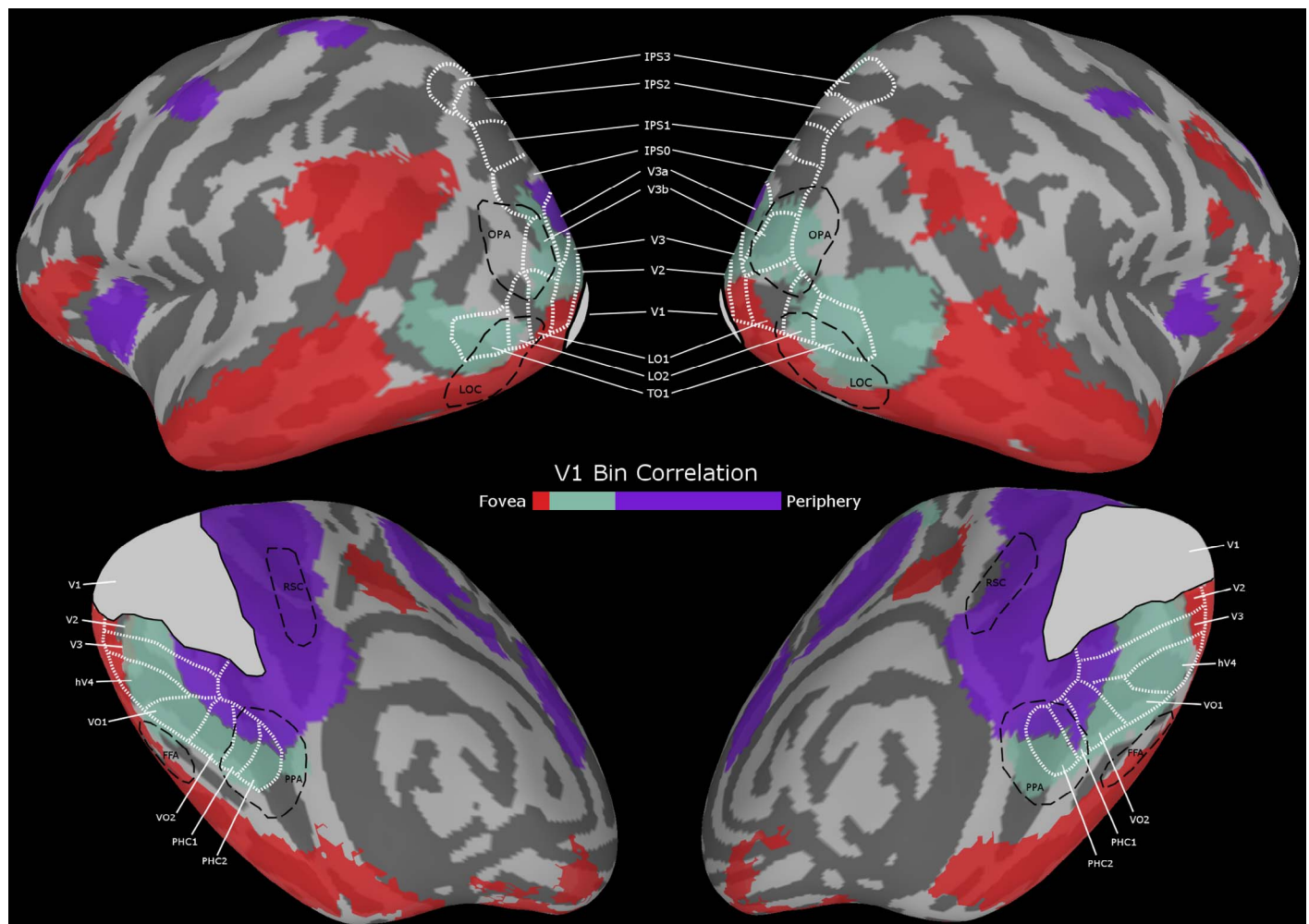


Figure 5. Comparison to a binning-based method. Rather than computing a full map over all V1 vertices, we binned each subject's vertices into three bins with equal numbers of vertices, representing the foveal, parafoveal, and peripheral visual field. A searchlight was then carried out to identify vertices showing a consistent connectivity preference for one of the bins ($q < 0.01$, minimum cluster size = 100 mm^2). This yielded results similar to those in Figure 3, though with reduced power.

more significant vertices, as well as a continuous measure of eccentricity preference (in degrees) rather than coarse bins. The binning results therefore validate our results regarding the large-scale eccentricity topographies across the cortex but also demonstrate that fitting full millimeter-scale weight maps can reveal details not visible in coarse bins.

Discussion

Using a specialized connectivity method, we measured the strength and specificity of functional connections between scene-sensitive regions and V1. Consistent with previous studies, this connectivity was largely biased toward V1's peripheral representation, but we also uncovered complex structure within and between scene regions. Although all regions of the

scene network showed evidence of a peripheral bias, the extent to which the regions preferentially connected to peripheral versus foveal V1 varied, with the weakest bias in OPA and strongest bias in RSC. Some regions, such as OPA and PHC1, showed strong connectivity to V1, whereas activity in RSC and aPPA could not be as easily predicted from V1 activity. Since our V1 map is limited to eccentricities within 15° , our measurement of V1 connectivity may underestimate how well peripheral V1 activity can predict these regions; that is, connectivity strength may improve if more peripheral V1 locations are included. However, it is not the case that a strong peripheral bias resulted more generally in poor connectivity strength; for example, PHC1 and PHC2 showed similar peripheral biases, but PHC1 had a higher V1 connectivity strength.

Activity in the OPA was strongly related to V1 activity and showed a bias away from the fovea, but peaked in connectivity around 10° of eccentricity. The

searchlight analysis (Figure 3) showed an interesting topography of eccentricity preferences around OPA: It overlaps with peripheral portions of several retinotopic maps from IPS0 to LO2, but also includes a foveal preference near the intersection of V3a, V3b, and IPS0. This matches the location of the V3a/b foveal representation (Larsson & Heeger, 2006), further validating that our functional connectivity analysis can reveal retinotopic biases consistent with traditional mapping approaches. Functionally, the relatively weak overall peripheral bias in OPA is consistent with proposals that OPA processes local scene properties that require relatively high acuity, such as spatial relationships between objects (Bettencourt & Xu, 2013), early processing of scene surfaces (Dilks, Julian, Paunov, & Kanwisher, 2013), or characteristic local features (Marchette, Vass, Ryan, & Epstein, 2015).

RSC showed the strongest peripheral biases out of all our ROIs, but was also less related to V1 (compared to OPA and posterior PPA). This suggests that RSC combines peripheral visual stimuli with many other sources of information from outside the visual system, as opposed to the more exclusively visual regions OPA and posterior PPA. In keeping with this, RSC is known to be involved in a wide range of cognitive tasks, including episodic memory, navigation, and imagination (Vann, Aggleton, & Maguire, 2009).

The PPA exhibited a strong gradient of V1 coupling along its anterior–posterior axis, replicating previous results by our group and others (Baldassano et al., 2013; Nasr, Devaney, & Tootell, 2013) and showing that these differences persist during free-viewing perception of natural movies. Posterior PPA (PHC1 and PHC2) showed a strong peripheral bias, consistent with the original description of these maps (Arcaro et al., 2009). We found that this peripheral bias extends into aPPA, but that the eccentricity profile in aPPA was much less consistent than in the more posterior subregions, suggesting that it is not as strongly tied to particular portions of V1. Together these results suggest that aPPA is still performing some processing of peripheral visual information but is less directly related to low-level visual features encoded in V1. This is consistent with a previous study of population receptive fields in posterior versus anterior PPA, which found that anterior PPA was less related to the specific position of a stimulus in the visual field (Silson, Chan, Reynolds, Kravitz, & Baker, 2015). These results join a broad set of converging evidence for a functional distinction between posterior and anterior PPA, with posterior PPA more related to low-level visual features (Aminoff & Tarr, 2015; Baldassano et al., 2016; Nasr, Echavarria, & Tootell, 2014; Watson, Hymers, Hartley, & Andrews, 2016) and anterior PPA more involved in global and memory-driven image properties (Aminoff & Tarr, 2015; Linsley & Macevoy, 2014; Marchette et

al., 2015; Park, Konkle, & Oliva, 2014; Watson et al., 2016).

The searchlight analyses showed that a peripheral eccentricity bias was also present throughout much of medial prefrontal cortex (mPFC). Since mPFC exhibits magnetoencephalography phase coupling with RSC (Kveraga et al., 2011), with which it also shares a structural connection (Greicius, Supekar, Menon, & Dougherty, 2009), its functional relationship with peripheral V1 is likely due to indirect connections through RSC. The mPFC has been proposed to serve a key role in the contextual association network, and is activated during contextual processing just like traditional scene regions (Aminoff, Schacter, & Bar, 2008; Peters, Daum, Gizewski, Forsting, & Suchan, 2009). It has therefore been proposed that mPFC integrates current visual information into a context frame (Kveraga et al., 2011). Our results support this view that contextual information from the peripheral visual field is integrated in mPFC.

Other smaller regions anterior to visual cortex also exhibited connectivity to specific eccentricities in V1. A broad section of the lateral temporal lobe was foveally connected, including the superior temporal sulcus, which is known to be functionally connected to the V1 fovea in macaques (Vincent et al., 2007) and to be involved in the foveal processing of faces (Haxby, Hoffman, & Gobbini, 2000). The peripherally connected patches near the central sulcus overlap with proposed topographic maps around the precentral sulcus and human frontal eye fields (Kastner et al., 2009), though our data do not show strong evidence of topographically organized eccentricities in this region. The functional role of the insula's peripheral bias is unclear, but this bias is consistent with previous studies that have also identified functional connectivity between the insula and the portion of the calcarine sulcus corresponding to peripheral V1 (Deen, Pitskel, & Pelphrey, 2011). The foveal connectivity in orbitofrontal cortex likely comes from its connections with the ventral temporal lobe, which have been identified both anatomically (Rolls, 2000) and functionally (Jackson, Hoffman, Pobric, & Lambon Ralph, 2016).

Conclusions

Topographic relationships between regions are a fundamental organizing principle of the brain (Jbabdi, Sotiropoulos, & Behrens, 2013). By examining millimeter-scale patterns of connections between V1 and scene-processing regions during free viewing of an audiovisual movie clip, we identified complex interactions between retinal eccentricity and functional

connectivity. Consistent with the known peripheral bias in scene perception (Larson & Loschky, 2009), we identified a bias in connectivity to peripheral V1 versus foveal V1 throughout well-known scene-sensitive regions and in other cortical regions including medial prefrontal cortex. We also identified differences among scene-sensitive regions, both in the strength of this peripheral bias and in the degree of coupling to signals in V1. OPA's peripheral bias was the least extreme, while RSC's was the most extreme, suggesting that these regions extract information from different portions of the visual field. Activity in OPA and posterior PPA (especially PHC1) was strongly related to V1 activity, while RSC and aPPA were less predictable from visual activity alone, suggesting that OPA and posterior PPA are closer to purely "visual" regions while RSC and aPPA are recruited by a more general set of cognitive functions. These results demonstrate that functional correlations during natural perception reflect eccentricity biases in high-level visual regions, and give insight into the fine-scale organization of the scene-processing network.

Keywords: fMRI, functional connectivity, eccentricity, periphery, receptive field, PPA, PHC, OPA, TOS, RSC, audiovisual

Acknowledgments

We thank Michael Arcaro, Sabine Kastner, Janice Chen, and Asieh Zadbood for providing the data and atlases used for this study. Funding was provided by the Office of Naval Research Multidisciplinary University Research Initiative (N000141410671).

Commercial relationships: none.

Corresponding author: Christopher Baldassano.

Email: chrisb@princeton.edu.

Address: Princeton Neuroscience Institute, Princeton University, Princeton, NJ, USA.

References

- Aminoff, E. M., Schacter, D. L., & Bar, M. (2008). The cortical underpinnings of context-based memory distortion. *Journal of Cognitive Neuroscience*, *20*(12), 2226–2237, doi:10.1162/jocn.2008.20156.
- Aminoff, E. M., & Tarr, M. J. (2015). Associative processing is inherent in scene perception. *PLoS ONE*, *10*(6), e0128840, doi:10.1371/journal.pone.0128840.
- Arcaro, M. J., Honey, C. J., Mruczek, R. E., Kastner, S., & Hasson, U. (2015). Widespread correlation patterns of fMRI signal across visual cortex reflect eccentricity organization. *eLife*, *4*, 1–28, doi:10.7554/eLife.03952.
- Arcaro, M. J., McMains, S. A., Singer, B. D., & Kastner, S. (2009). Retinotopic organization of human ventral visual cortex. *The Journal of Neuroscience*, *29*(34), 10638–10652, doi:10.1523/JNEUROSCI.2807-09.2009.
- Baldassano, C., Beck, D. M., & Fei-Fei, L. (2013). Differential connectivity within the Parahippocampal Place Area. *NeuroImage*, *75*, 228–237, doi:10.1016/j.neuroimage.2013.02.073.
- Baldassano, C., Beck, D. M., & Fei-Fei, L. (2015). Parcellating connectivity in spatial maps. *PeerJ*, *3*, e784, doi:10.7717/peerj.784.
- Baldassano, C., Beck, D. M., & Fei-Fei, L. (2016). Human-object interactions are more than the sum of their parts. *Cerebral Cortex*, in press, doi:10.1093/cercor/bhw077.
- Baldassano, C., Jordan, M. C., Beck, D. M., & Fei-Fei, L. (2012). Voxel-level functional connectivity using spatial regularization. *NeuroImage*, *63*(3), 1099–1106, doi:10.1016/j.neuroimage.2012.07.046.
- Bettencourt, K. C., & Xu, Y. (2013). The role of transverse occipital sulcus in scene perception and its relationship to object individuation in inferior intraparietal sulcus. *Journal of Cognitive Neuroscience*, *25*, 1711–1722, doi:10.1162/jocn_a_00422.
- Bock, A. S., Binda, P., Benson, N. C., Bridge, H., Watkins, K. E., & Fine, I. (2015). Resting-state retinotopic organization in the absence of retinal input and visual experience. *The Journal of Neuroscience*, *35*(36), 12366–12382, doi:10.1523/JNEUROSCI.4715-14.2015.
- Boucart, M., Moroni, C., Thibaut, M., Szaffarczyk, S., & Greene, M. (2013). Scene categorization at large visual eccentricities. *Vision Research*, *86*, 35–42, doi:10.1016/j.visres.2013.04.006.
- Butt, O. H., Benson, N. C., Datta, R., & Aguirre, G. K. (2013). The fine-scale functional correlation of striate cortex in sighted and blind people. *The Journal of Neuroscience*, *33*(41), 16209–16219, doi:10.1523/JNEUROSCI.0363-13.2013.
- Cox, R. W. (1996). AFNI: Software for analysis and visualization of functional magnetic resonance neuroimages. *Computers and Biomedical Research*, *29*(3), 162–173. <http://www.ncbi.nlm.nih.gov/pubmed/8812068>
- Chen, J., Honey, C. J., Simony, E., Arcaro, M. J., Norman, K. A., & Hasson, U. (2015). Accessing real-life episodic information from minutes versus hours earlier modulates hippocampal and high-

- order cortical dynamics. *Cerebral Cortex*, in press, doi:10.1093/cercor/bhv155.
- Chen, J., Leong, Y. C., Norman, K. A., & Hasson, U. (2016). Shared experience, shared memory: a common structure for brain activity during naturalistic recall. *bioRxiv*, preprint, doi:10.1101/035931.
- Dale, A. M., Fischl, B., & Sereno, M. I. (1999). Cortical surface-based analysis: I. Segmentation and surface reconstruction. *NeuroImage*, 9(2), 179–194, doi:10.1006/nimg.1998.0395.
- Deen, B., Pitskel, N. B., & Pelphrey, K. A. (2011). Three systems of insular functional connectivity identified with cluster analysis. *Cerebral Cortex*, 21(7), 1498–1506, doi:10.1093/cercor/bhq186.
- Dilks, D. D., Julian, J. B., Paunov, A. M., & Kanwisher, N. (2013). The occipital place area is causally and selectively involved in scene perception. *The Journal of Neuroscience*, 33(4), 1331–1336, doi:10.1523/JNEUROSCI.4081-12.2013.
- Epstein, R. A. (2014). Neural systems for visual scene recognition. In M. Bar & K. Kveraga (Eds.), *Scene vision* (pp. 105–134). Cambridge, MA: MIT Press.
- Fischl, B., Sereno, M. I., & Dale, A. M. (1999). Cortical surface-based analysis: II. Inflation, flattening, and a surface-based coordinate system. *NeuroImage*, 9(2), 195–207, doi:10.1006/nimg.1998.0396.
- Fox, M. D., Zhang, D., Snyder, A. Z., & Raichle, M. E. (2009). The global signal and observed anticorrelated resting state brain networks. *Journal of Neurophysiology*, 101(6), 3270–3283, doi:10.1152/jn.90777.2008.
- Goesaert, E., & Op de Beeck, H. P. (2010). Continuous mapping of the cortical object vision pathway using traveling waves in object space. *NeuroImage*, 49(4), 3248–3256, doi:10.1016/j.neuroimage.2009.11.036.
- Greicius, M. D., Supekar, K., Menon, V., & Dougherty, R. F. (2009). Resting-state functional connectivity reflects structural connectivity in the default mode network. *Cerebral Cortex*, 19(1), 72–78, doi:10.1093/cercor/bhn059.
- Haak, K. V., Winawer, J., Harvey, B. M., Renken, R., Dumoulin, S. O., Wandell, B. A., & Cornelissen, F. W. (2013). Connective field modeling. *NeuroImage*, 66, 376–384, doi:10.1016/j.neuroimage.2012.10.037.
- Hasson, U., Levy, I., Behrmann, M., Hendler, T., & Malach, R. (2002). Eccentricity bias as an organizing principle for human high-order object areas. *Neuron*, 34(3), 479–490. <http://www.ncbi.nlm.nih.gov/pubmed/11988177>
- Haxby, J. V., Hoffman, E. A., & Gobbini, M. I. (2000). The distributed human neural system for face perception. *Trends in Cognitive Sciences*, 4(6), 223–233, doi:10.1016/S1364-6613(00)01482-0.
- Heinzle, J., Kahnt, T., & Haynes, J. D. (2011). Topographically specific functional connectivity between visual field maps in the human brain. *NeuroImage*, 56(3), 1426–1436, doi:10.1016/j.neuroimage.2011.02.077.
- Huang, R.-S., & Sereno, M. I. (2013). Bottom-up retinotopic organization supports top-down mental imagery. *The Open Neuroimaging Journal*, 7(858), 58–67, doi:10.2174/1874440001307010058.
- Jackson, R. L., Hoffman, P., Pobric, G., & Lambon Ralph, M. A. (2016). The semantic network at work and rest: Differential connectivity of anterior temporal lobe subregions. *The Journal of Neuroscience*, 36(5), 1490–1501, doi:10.1523/JNEUROSCI.2999-15.2016.
- Jbabdi, S., Sotiropoulos, S. N., & Behrens, T. E. (2013). The topographic connectome. *Current Opinion in Neurobiology*, 23(2), 207–215, doi:10.1016/j.conb.2012.12.004.
- Kanwisher, N. (2001). Faces and places: Of central (and peripheral) interest. *Nature Neuroscience*, 4(5), 455–456, doi:10.1038/87399.
- Kastner, S., Desimone, K., Konen, C. S., Szczepanski, S. M., Weiner, K. S., Schneider, K. A., & Chun, M. (2009). Topographic maps in human frontal cortex revealed in memory-guided saccade and spatial working-memory tasks. *Journal of Neurophysiology*, 97(5), 3494–3507, doi:10.1152/jn.00010.2007.
- Kveraga, K., Ghuman, A. S., Kassam, K. S., Aminoff, E. A., Hämäläinen, M. S., Chaumon, M., & Bar, M. (2011). Early onset of neural synchronization in the contextual associations network. *Proceedings of the National Academy of Sciences, USA*, 108, 3389–3394, doi:10.1073/pnas.1013760108.
- Larson, A. M., Freeman, T. E., Ringer, R. V., & Loschky, L. C. (2014). The spatiotemporal dynamics of scene gist recognition. *Journal of Experimental Psychology: Human Perception and Performance*, 40(2), 471–487, doi:10.1037/a0034986.
- Larson, A. M., & Loschky, L. C. (2009). The contributions of central versus peripheral vision to scene gist recognition. *Journal of Vision*, 9(10):6, 1–16, doi:10.1167/9.10.6. [PubMed] [Article]
- Larsson, J., & Heeger, D. J. (2006). Two retinotopic visual areas in human lateral occipital cortex. *The Journal of Neuroscience*, 26(51), 13128–13142, doi:10.1523/JNEUROSCI.1657-06.2006.
- Levy, I., Hasson, U., Avidan, G., Hendler, T., & Malach, R. (2001). Center-periphery organization

- of human object areas. *Nature Neuroscience*, 4(5), 533–539, doi:10.1038/87490.
- Linsley, D., & Macevoy, S. P. (2014). Encoding-stage crosstalk between object- and spatial property-based scene processing pathways. *Cerebral Cortex*, 25(8), 2267–2281, doi:10.1093/cercor/bhu034.
- Malach, R., Levy, I., & Hasson, U. (2002). The topography of high-order human object areas. *Trends in Cognitive Sciences*, 6(4), 176–184, doi:10.1016/S1364-6613(02)01870-3.
- Marchette, S. A., Vass, L. K., Ryan, J., & Epstein, R. A. (2015). Outside looking in: Landmark generalization in the human navigational system. *The Journal of Neuroscience*, 35(44), 14896–14908, doi:10.1523/JNEUROSCI.2270-15.2015.
- Mruczek, R. E. B., von Loga, I. S., & Kastner, S. (2013). The representation of tool and non-tool object information in the human intraparietal sulcus. *Journal of Neurophysiology*, 109(12), 2883–2896, doi:10.1152/jn.00658.2012.
- Murphy, K., Birn, R. M., Handwerker, D. A., Jones, T. B., & Bandettini, P. A. (2009). The impact of global signal regression on resting state correlations: Are anti-correlated networks introduced? *NeuroImage*, 44(3), 893–905, doi:10.1016/j.neuroimage.2008.09.036.
- Nasr, S., Devaney, K. J., & Tootell, R. B. H. (2013). Spatial encoding and underlying circuitry in scene-selective cortex. *NeuroImage*, 83, 892–900, doi:10.1016/j.neuroimage.2013.07.030.
- Nasr, S., Echavarria, C. E., & Tootell, R. B. H. (2014). Thinking outside the box: rectilinear shapes selectively activate scene-selective cortex. *The Journal of Neuroscience*, 34(20), 6721–6735, doi:10.1523/JNEUROSCI.4802-13.2014.
- Park, S., Konkle, T., & Oliva, A. (2014). Parametric coding of the size and clutter of natural scenes in the human brain. *Cerebral Cortex*, 25(7), 1792–1805, doi:10.1093/cercor/bht418.
- Peters, J., Daum, I., Gizewski, E., Forsting, M., & Suchan, B. (2009). Associations evoked during memory encoding recruit the context-network. *Hippocampus*, 19(2), 141–151, doi:10.1002/hipo.20490.
- Regev, M., Honey, C. J., Simony, E., & Hasson, U. (2013). Selective and invariant neural responses to spoken and written narratives. *The Journal of Neuroscience*, 33(40), 15978–15988, doi:10.1523/JNEUROSCI.1580-13.2013.
- Rolls, E. T. (2000). The orbitofrontal cortex and reward. *Cerebral Cortex*, 10(3), 284–294, doi:10.1093/cercor/10.3.284.
- Silson, E. H., Chan, A. W.-Y., Reynolds, R. C., Kravitz, D. J., & Baker, C. I. (2015). A retinotopic basis for the division of high-level scene processing between lateral and ventral human occipitotemporal cortex. *The Journal of Neuroscience*, 35(34), 11921–11935, doi:10.1523/JNEUROSCI.0137-15.2015.
- Swisher, J. D., Halko, M. A., Merabet, L. B., McMains, S. A., & Somers, D. C. (2007). Visual topography of human intraparietal sulcus. *The Journal of Neuroscience*, 27(20), 5326–5337, doi:10.1523/JNEUROSCI.0991-07.2007.
- Vann, S. D., Aggleton, J. P., & Maguire, E. A. (2009). What does the retrosplenial cortex do? *Nature Reviews Neuroscience*, 10(11), 792–802, doi:10.1038/nrn2733.
- Vincent, J. L., Patel, G. H., Fox, M. D., Snyder, A. Z., Baker, J. T., Van Essen, D. C., & Raichle, M. E. (2007). Intrinsic functional architecture in the anaesthetized monkey brain. *Nature*, 447(7140), 83–86, doi:10.1038/nature05758.
- Wang, L., Mruczek, R. E. B., Arcaro, M. J., & Kastner, S. (2014). Probabilistic maps of visual topography in human cortex. *Cerebral Cortex*, 25(10), 3911–3931, doi:10.1093/cercor/bhu277.
- Watson, D. M., Hymers, M., Hartley, T., & Andrews, T. J. (2016). Patterns of neural response in scene-selective regions of the human brain are affected by low-level manipulations of spatial frequency. *NeuroImage*, 124, 107–117, doi:10.1016/j.neuroimage.2015.08.058.